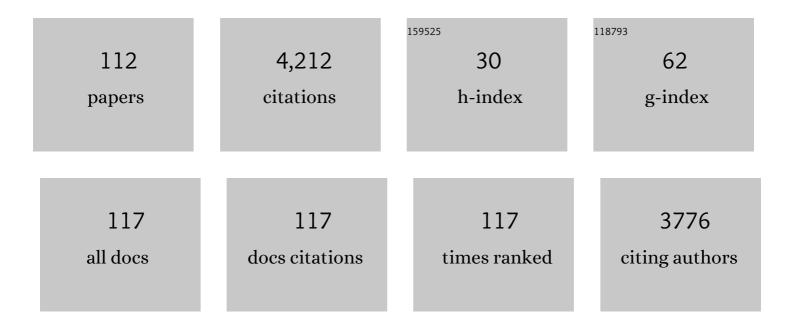


## List of Publications by Year in descending order

Source: https://exaly.com/author-pdf/2145534/publications.pdf Version: 2024-02-01



#	Article	IF	CITATIONS
1	Magnitude and Role of Wall Shear Stress on Cerebral Aneurysm. Stroke, 2004, 35, 2500-2505.	1.0	704
2	Incomplete Stent Apposition Causes High Shear Flow Disturbances and Delay in Neointimal Coverage as a Function of Strut to Wall Detachment Distance. Circulation: Cardiovascular Interventions, 2014, 7, 180-189.	1.4	178
3	Expert recommendations on the assessment of wall shear stress in human coronary arteries: existing methodologies, technical considerations, and clinical applications. European Heart Journal, 2019, 40, 3421-3433.	1.0	178
4	Fluid–structure Interaction Modeling of Aneurysmal Conditions with High and Normal Blood Pressures. Computational Mechanics, 2006, 38, 482-490.	2.2	164
5	Influence of wall elasticity in patient-specific hemodynamic simulations. Computers and Fluids, 2007, 36, 160-168.	1.3	154
6	Computer modeling of cardiovascular fluid–structure interactions with the deforming-spatial-domain/stabilized space–time formulation. Computer Methods in Applied Mechanics and Engineering, 2006, 195, 1885-1895.	3.4	152
7	Fluid–structure interaction modeling of a patient-specific cerebral aneurysm: influence of structural modeling. Computational Mechanics, 2008, 43, 151-159.	2.2	147
8	Fluid–structure interaction modeling of blood flow and cerebral aneurysm: Significance of artery and aneurysm shapes. Computer Methods in Applied Mechanics and Engineering, 2009, 198, 3613-3621.	3.4	139
9	Impact of stent strut design in metallic stents and biodegradable scaffolds. International Journal of Cardiology, 2014, 177, 800-808.	0.8	136
10	Computational Fluid Dynamic Analysis of the Left Atrial Appendage to Predict Thrombosis Risk. Frontiers in Cardiovascular Medicine, 2018, 5, 34.	1.1	112
11	Fluid–structure interaction analysis of a patientâ€specific right coronary artery with physiological velocity and pressure waveforms. Communications in Numerical Methods in Engineering, 2009, 25, 565-580.	1.3	111
12	Kissing Balloon or Sequential Dilation of the Side Branch and Main Vessel for Provisional Stenting of Bifurcations. JACC: Cardiovascular Interventions, 2012, 5, 47-56.	1.1	111
13	Role of the Bloodstream Impacting Force and the Local Pressure Elevation in the Rupture of Cerebral Aneurysms. Stroke, 2005, 36, 1933-1938.	1.0	101
14	Vulnerable plaques and patients: state-of-the-art. European Heart Journal, 2020, 41, 2997-3004.	1.0	98
15	Finite element simulation of blood flow in the cerebral artery. Computer Methods in Applied Mechanics and Engineering, 2001, 191, 661-671.	3.4	85
16	Influence of wall thickness on fluid–structure interaction computations of cerebral aneurysms. International Journal for Numerical Methods in Biomedical Engineering, 2010, 26, 336-347.	1.0	82
17	Numerical investigation of the effect of hypertensive blood pressure on cerebral aneurysm—Dependence of the effect on the aneurysm shape. International Journal for Numerical Methods in Fluids, 2007, 54, 995-1009.	0.9	80
18	Local Hemodynamic Forces After Stenting. Arteriosclerosis, Thrombosis, and Vascular Biology, 2017, 37, 2231-2242.	1.1	78

#	Article	IF	CITATIONS
19	Location of side branch access critically affects results in bifurcation stenting: Insights from bench modeling and computational flow simulation. International Journal of Cardiology, 2013, 168, 3623-3628.	0.8	63
20	Role of 0D peripheral vasculature model in fluid–structure interaction modeling of aneurysms. Computational Mechanics, 2010, 46, 43-52.	2.2	60
21	Influencing factors in imageâ€based fluid–structure interaction computation of cerebral aneurysms. International Journal for Numerical Methods in Fluids, 2011, 65, 324-340.	0.9	53
22	Influence of Wall Elasticity on Image-Based Blood Flow Simulations. Nihon Kikai Gakkai Ronbunshu, A Hen/Transactions of the Japan Society of Mechanical Engineers, Part A, 2004, 70, 1224-1231.	0.2	50
23	Crush, Culotte, T and Protrusion: Which 2-Stent Technique for Treatment of True Bifurcation Lesions?. Circulation Journal, 2013, 77, 73-80.	0.7	47
24	Estimation of element-based zero-stress state for arterial FSI computations. Computational Mechanics, 2014, 54, 895-910.	2.2	47
25	Computational Modeling of LDL and Albumin Transport in an In Vivo CT Image-Based Human Right Coronary Artery. Journal of Biomechanical Engineering, 2009, 131, 021003.	0.6	46
26	Coronary arterial dynamics computation with medical-image-based time-dependent anatomical models and element-based zero-stress state estimates. Computational Mechanics, 2014, 54, 1047-1053.	2.2	43
27	MR Image-Based Geometric and Hemodynamic Investigation of the Right Coronary Artery with Dynamic Vessel Motion. Annals of Biomedical Engineering, 2010, 38, 2606-2620.	1.3	42
28	Integrated morphologic and functional assessment of the aortic root after different tissue valve root replacement procedures. Journal of Thoracic and Cardiovascular Surgery, 2012, 143, 1422-1428.e2.	0.4	38
29	Endothelial shear stress 5 years after implantation of a coronary bioresorbable scaffold. European Heart Journal, 2018, 39, 1602-1609.	1.0	33
30	A Mock Circulatory System Incorporating a Compliant 3Dâ€Printed Anatomical Model to Investigate Pulmonary Hemodynamics. Artificial Organs, 2017, 41, 637-646.	1.0	31
31	The Nidus for Possible ThrombusÂFormation. JACC: Cardiovascular Interventions, 2016, 9, 2167-2168.	1.1	30
32	A Technical Review of Minimally Invasive Mitral Valve Replacements. Cardiovascular Engineering and Technology, 2015, 6, 174-184.	0.7	28
33	Vulnerable plaque detection: an unrealistic quest or a feasible objective with a clinical value?. Heart, 2016, 102, 581-589.	1.2	27
34	Shear Stress Estimated by Quantitative Coronary Angiography Predicts Plaques Prone to Progress and Cause Events. JACC: Cardiovascular Imaging, 2020, 13, 2206-2219.	2.3	27
35	Stress phase angle depicts differences in coronary artery hemodynamics due to changes in flow and geometry after percutaneous coronary intervention. American Journal of Physiology - Heart and Circulatory Physiology, 2009, 296, H765-H776.	1.5	26
36	Patient-Specific Modeling and Multi-Scale Blood Simulation for Computational Hemodynamic Study on the Human Cerebrovascular System. Current Pharmaceutical Biotechnology, 2012, 13, 2153-2165.	0.9	24

#	Article	IF	CITATIONS
37	A Computationally Efficient Approach to Segmentation of the Aorta and Coronary Arteries Using Deep Learning. IEEE Access, 2021, 9, 108873-108888.	2.6	24
38	Strut protrusion and shape impact on endothelial shear stress: insights from pre-clinical study comparing Mirage and Absorb bioresorbable scaffolds. International Journal of Cardiovascular Imaging, 2017, 33, 1313-1322.	0.7	23
39	Modelling of inflow boundary conditions for image-based simulation of cerebrovascular flow. International Journal for Numerical Methods in Fluids, 2005, 47, 603-617.	0.9	22
40	A computational study on the influence of catheter-delivered intravascular probes on blood flow in a coronary artery model. Journal of Biomechanics, 2007, 40, 2501-2509.	0.9	22
41	Wall shear stress estimated by 3D-QCA can predict cardiovascular events in lesions with borderline negative fractional flow reserve. Atherosclerosis, 2021, 322, 24-30.	0.4	21
42	Comparison of Aortic Flow Patterns Before and After Transcatheter Aortic Valve Implantation. Cardiovascular Engineering and Technology, 2012, 3, 123-135.	0.7	20
43	Biodegradable vascular scaffold: is optimal expansion the key to minimising flow disturbances and risk of adverse events?. EuroIntervention, 2015, 10, 1139-1142.	1.4	19
44	Aortic root dynamism, geometry, and function after the remodeling operation: Clinical relevance. Journal of Thoracic and Cardiovascular Surgery, 2018, 156, 951-962.e2.	0.4	18
45	Disturbed Flow in a Stenosed Carotid Artery Bifurcation: Comparison of RANS-Based Transitional Model and LES with Experimental Measurements. International Journal of Applied Mechanics, 2019, 11, 1950032.	1.3	17
46	Implications of the local hemodynamic forces on the formation and destabilization of neoatherosclerotic lesions. International Journal of Cardiology, 2018, 272, 7-12.	0.8	16
47	Intravascular multimodality imaging: feasibility and role in the evaluation of coronary plaque pathology. European Heart Journal Cardiovascular Imaging, 2017, 18, 613-620.	0.5	16
48	Difference in haemodynamic microenvironment in vessels scaffolded with Absorb BVS and Mirage BRMS: insights from a preclinical endothelial shear stress study. EuroIntervention, 2017, 13, 1327-1335.	1.4	16
49	On outflow boundary conditions for CT-based computation of FFR: Examination using PET images. Medical Engineering and Physics, 2020, 76, 79-87.	0.8	15
50	Early coverage of drug-eluting stents analysed by optical coherence tomography: evidence of the impact of stent apposition and strut characteristics on the neointimal healing process. EuroIntervention, 2016, 12, e605-e614.	1.4	15
51	Preclinical assessment of the endothelial shear stress in porcine-based models following implantation of two different bioresorbable scaffolds: effect of scaffold design on the local haemodynamic micro-environment. EuroIntervention, 2016, 12, 1296-1296.	1.4	15
52	Numerical Simulation System for Blood Flow in the Cerebral Artery Using CT Imaging Data. JSME International Journal Series C-Mechanical Systems Machine Elements and Manufacturing, 2001, 44, 982-989.	0.3	14
53	Patient-Specific Coronary Stenoses Can Be Modeled Using a Combination of OCT and Flow Velocities to Accurately Predict Hyperemic Pressure Gradients. IEEE Transactions on Biomedical Engineering, 2014, 61, 1902-1913.	2.5	14
54	Design, Analysis and Testing of a Novel Mitral Valve for Transcatheter Implantation. Annals of Biomedical Engineering, 2017, 45, 1852-1864.	1.3	14

#	Article	IF	CITATIONS
55	Implications of the local haemodynamic forces on the phenotype of coronary plaques. Heart, 2019, 105, 1078-1086.	1.2	14
56	Impact of Inflow Boundary Conditions on the Calculation of CT-Based FFR. Fluids, 2019, 4, 60.	0.8	14
57	Advanced deep learning methodology for accurate, real-time segmentation of high-resolution intravascular ultrasound images. International Journal of Cardiology, 2021, 339, 185-191.	0.8	14
58	Assessment of the hemodynamic characteristics of Absorb BVS in a porcine coronary artery model. International Journal of Cardiology, 2017, 227, 467-473.	0.8	13
59	Two Secreted Proteoglycans, Activators of Urothelial Cell–Cell Adhesion, Negatively Contribute to Bladder Cancer Initiation and Progression. Cancers, 2020, 12, 3362.	1.7	13
60	Computerised Methodologies for Non-Invasive Angiography-Derived Fractional Flow Reserve Assessment: A Critical Review. Journal of Interventional Cardiology, 2020, 2020, 1-10.	0.5	13
61	Neointima and neoatherosclerotic characteristics in bare metal and first- and second-generation drug-eluting stents in patients admitted with cardiovascular events attributed to stent failure: an optical coherence tomography study. EuroIntervention, 2018, 13, e1831-e1840.	1.4	13
62	Predicting Impending Rupture of the Ascending Aorta With Bicuspid Aortic Valve. JACC: Cardiovascular Imaging, 2013, 6, 1017-1019.	2.3	12
63	Modelling multi-scale cell–tissue interaction of tissue-engineered muscle constructs. Journal of Tissue Engineering, 2018, 9, 204173141878714.	2.3	12
64	Bioresorbable vascular scaffold radial expansion and conformation compared to a metallic platform: insights from in vitro expansion in a coronary artery lesion model. EuroIntervention, 2016, 12, 834-844.	1.4	12
65	Midterm results of the Ross procedure in children: an appraisal of the subannular implantation with interrupted sutures techniqueâ€. European Journal of Cardio-thoracic Surgery, 2017, 52, 798-804.	0.6	11
66	Angiographic derived endothelial shear stress: a new predictor of atherosclerotic disease progression. European Heart Journal Cardiovascular Imaging, 2019, 20, 314-322.	0.5	11
67	The Evolution of Data Fusion Methodologies Developed to Reconstruct Coronary Artery Geometry From Intravascular Imaging and Coronary Angiography Data: A Comprehensive Review. Frontiers in Cardiovascular Medicine, 2020, 7, 33.	1.1	11
68	A deep learning methodology for the automated detection of end-diastolic frames in intravascular ultrasound images. International Journal of Cardiovascular Imaging, 2021, 37, 1825-1837.	0.7	11
69	Post-implantation shear stress assessment: an emerging tool for differentiation of bioresorbable scaffolds. International Journal of Cardiovascular Imaging, 2019, 35, 409-418.	0.7	10
70	Left Ventricular Assist Device Flow Pattern Analysis Using a Novel Model Incorporating Left Ventricular Pulsatility. ASAIO Journal, 2021, 67, 724-732.	0.9	10
71	Evaluation of the Efficacy of Computed Tomographic Coronary Angiography in Assessing Coronary Artery Morphology and Physiology: Rationale and Study Design. Cardiology, 2020, 145, 285-293.	0.6	9
72	Numerical evaluation of elastic models in blood flow–arterial wall interaction. International Journal of Computational Fluid Dynamics, 2006, 20, 223-228.	0.5	8

#	Article	IF	CITATIONS
73	The Effect of Strut Protrusion on Shear Stress Distribution. JACC: Cardiovascular Interventions, 2017, 10, 1803-1805.	1.1	8
74	Non-Newtonian pulsatile shear stress assessment: a method to differentiate bioresorbable scaffold platforms. European Heart Journal, 2017, 38, 2570-2570.	1.0	7
75	Reliable in vivo intravascular imaging plaque characterization: A challenge unmet. American Heart Journal, 2019, 218, 20-31.	1.2	7
76	Low-Cost Fabrication of Polyvinyl Alcohol-Based Personalized Vascular Phantoms for In Vitro Hemodynamic Studies: Three Applications. Journal of Engineering and Science in Medical Diagnostics and Therapy, 2020, 3, .	0.3	7
77	Intravascular imaging assessment of pharmacotherapies targeting atherosclerosis: advantages and limitations in predicting their prognostic implications. Cardiovascular Research, 2023, 119, 121-135.	1.8	7
78	Computational biomechanics of the aortic root. Aswan Heart Centre Science & Practice Series, 2011, 2011, .	0.3	6
79	Predictive value of the QFR in detecting vulnerable plaques in non-flow limiting lesions: a combined analysis of the PROSPECT and IBIS-4 study. International Journal of Cardiovascular Imaging, 2020, 36, 993-1002.	0.7	6
80	Use of quantitative cardiovascular magnetic resonance myocardial perfusion mapping for characterization of ischemia in patients with left internal mammary coronary artery bypass grafts. Journal of Cardiovascular Magnetic Resonance, 2021, 23, 82.	1.6	6
81	Enhancing Magnetic Resonance Imaging With Computational Fluid Dynamics. Journal of Engineering and Science in Medical Diagnostics and Therapy, 2019, 2, .	0.3	6
82	Five-year follow-up of underexpanded and overexpanded bioresorbable scaffolds: self-correction and impact on shear stress. EuroIntervention, 2017, 12, 2158-2159.	1.4	6
83	<scp>H</scp> emodynamic analysis of a novel bioresorbable scaffold in porcine coronary artery model. Catheterization and Cardiovascular Interventions, 2018, 91, 1084-1091.	0.7	5
84	The impact of plaque type on strut embedment/protrusion and shear stress distribution in bioresorbable scaffold. European Heart Journal Cardiovascular Imaging, 2020, 21, 454-462.	0.5	5
85	Efficacy and Reproducibility of Attenuation-Compensated Optical Coherence Tomography for Assessing External Elastic Membrane Border and Plaque Composition in Native and Stented Segments ― An In Vivo and Histology-Based Study ―. Circulation Journal, 2019, 84, 91-100.	0.7	5
86	Angiography-Based 4-Dimensional Superficial Wall Strain and Stress: A New Diagnostic Tool in the Catheterization Laboratory. Frontiers in Cardiovascular Medicine, 2021, 8, 667310.	1.1	5
87	Dynamic Characterisation of Fibre-Optic Temperature Sensors for Physiological Monitoring. Sensors, 2021, 21, 221.	2.1	5
88	Impact of bioresorbable scaffold design characteristics on local haemodynamic forces: an ex vivo assessment with computational fluid dynamics simulations. EuroIntervention, 2020, 16, e930-e937.	1.4	5
89	An integrated geometric modelling framework for patient-specific computational haemodynamic study on wide-ranged vascular network. Computer Methods in Biomechanics and Biomedical Engineering, 2012, 15, 615-625.	0.9	4
90	Failure and detachment path of impulsively loaded plates. Thin-Walled Structures, 2020, 155, 106871.	2.7	4

#	Article	IF	CITATIONS
91	Early strut protrusion and late neointima thickness in the Absorb bioresorbable scaffold: a serial wall shear stress analysis up to five years. EuroIntervention, 2019, 15, e370-e379.	1.4	4
92	Machine learning for atherosclerotic tissue component classification in combined near-infrared spectroscopy intravascular ultrasound imaging: Validation against histology. Atherosclerosis, 2022, 345, 15-25.	0.4	4
93	An automated software for real-time quantification of wall shear stress distribution in quantitative coronary angiography data. International Journal of Cardiology, 2022, , .	0.8	4
94	Spatiotemporal droplet dispersion measurements demonstrate face masks reduce risks from singing. Scientific Reports, 2021, 11, 24183.	1.6	4
95	Method for Percutaneously Introducing, and Removing, Anatomical Stenosis of Predetermined Severity In Vivo: The "Stenotic Stent― Journal of Cardiovascular Translational Research, 2013, 6, 640-648.	1.1	3
96	Characterisation of spatiotemporal aortic flow and aortic wall biomechanics in coarctation. Global Cardiology Science & Practice, 2015, 2015, 45.	0.3	3
97	The effect of strut thickness on shear stress distribution in a preclinical model. International Journal of Cardiovascular Imaging, 2017, 33, 1675-1676.	0.7	3
98	Endothelial shear stress and vascular remodeling in bioresorbable scaffold and metallic stent. Atherosclerosis, 2020, 312, 79-89.	0.4	3
99	Endâ€diastolic segmentation of intravascular ultrasound images enables more reproducible volumetric analysis of atheroma burden. Catheterization and Cardiovascular Interventions, 2022, 99, 706-713.	0.7	3
100	One-year performance of biorestorative polymeric coronary bypass grafts in an ovine model: correlation between early biomechanics and late serial Quantitative Flow Ratio. European Journal of Cardio-thoracic Surgery, 2022, 61, 1402-1411.	0.6	3
101	Quantitative assessment of right ventricular structure and flow dynamics in pulmonary homograft obstruction. Global Cardiology Science & Practice, 2014, 2014, 47.	0.3	2
102	Local Hemodynamics. JACC: Cardiovascular Interventions, 2015, 8, e149-e150.	1.1	2
103	Importance of Stress Mapping of Aortic Wall inÂAortic Valve Disease. Journal of the American College of Cardiology, 2016, 67, 1755-1756.	1.2	2
104	Experimental Validation of Enhanced Magnetic Resonance Imaging (EMRI) Using Particle Image Velocimetry (PIV). Annals of Biomedical Engineering, 2021, , 1.	1.3	2
105	CT-based fractional flow reserve: development and expanded application. Global Cardiology Science & Practice, 2021, 2021, e202120.	0.3	2
106	Uncovered non-apposed side-branch struts in a bifurcation lesion: aÂnidus for late stent thrombosis. Hellenic Journal of Cardiology, 2021, 63, 96-96.	0.4	1
107	Estimation of Smoothing Error in Applying the Computed Tomography to Hemodynamic Numerical Simulations. The Proceedings of the JSME Annual Meeting, 2000, 2000.1, 261-262.	0.0	1
108	Preclinical evaluation of a thin-strut bioresorbable scaffold (ArterioSorb): acute-phase invasive imaging assessment and hemodynamic implication EuroIntervention, 2020, 16, e141-e146.	1.4	1

#	Article	IF	CITATIONS
109	Morphological and Physiological Characteristics of Ruptured Plaques in Native Arteries and Neoatherosclerotic Segments: An OCT-Based and Computational Fluid Dynamics Study. Frontiers in Cardiovascular Medicine, 2022, 9, .	1.1	1
110	F-0819 Fluid Structure Interaction Analysis of Curved Pipe Similar to Internal Carotid Artery. The Proceedings of the JSME Annual Meeting, 2001, IV.01.1, 37-38.	0.0	0
111	1B43 Fluid-Structure Interaction Analysis of Growth of Cerebral Aneurysm. Proceedings of the JSME Bioengineering Conference and Seminar, 2001, 2001.12, 71-72.	0.0	Ο
112	Abstract 19508: Mid-term Results of the Ross Procedure in Children: A Reappraisal of the Subannular Implantation Technique. Circulation, 2015, 132, .	1.6	0